Colloids and Surfaces B: Biointerfaces 208 (2021) 112048

Contents lists available at ScienceDirect

Colloids and Surfaces B: Biointerfaces

journal homepage: www.elsevier.com/locate/colsurfb

Indocyanine green-carrying polymeric nanoparticles with acid-triggered detachable PEG coating and drug release for boosting cancer photothermal therapy

Chih-Wei Ting, Ya-Hsuan Chou, Shih-Yu Huang, Wen-Hsuan Chiang *

Department of Chemical Engineering, National Chung Hsing University, Taichung, 402, Taiwan

ARTICLE INFO

Keywords:
Indocyanine green
Cancer photothermal therapy
Acid-triggered PEG detachment
Controlled drug release
Hybrid polymeric nanoparticles

ABSTRACT

In order to boost anticancer efficacy of indocyanine green (ICG)-mediated photothermal therapy (PTT) by promoting intracellular ICG delivery, the ICG-carrying hybrid polymeric nanoparticles were fabricated in this study by co-assembly of hydrophobic poly(lactic-co-glycolic acid) (PLGA) segments, ICG molecules, amphiphilic tocopheryl polyethylene glycol succinate (TPGS) and pH-responsive methoxy poly(ethylene glycol)-benzoic imine-1-octadecanamine (mPEG-b-C18) segments in aqueous solution. The ICG-loaded nanoparticles were characterized to have ICG-containing PLGA core stabilized by hydrophilic PEG-rich surface coating and a well-dispersed spherical shape. Moreover, the ICG-loaded nanoparticles in pH 7.4 aqueous solution sufficiently inhibited ICG self-aggregation and leakage, thereby increasing aqueous photostability of ICG molecules. Notably, when the solution pH was reduced from pH 7.4–5.5, the acid-triggered hydrolysis of benzoic-imine linkers within mPEG-b-C18 remarkably facilitated the detachment of mPEG segments from ICG-loaded nanoparticles, thus accelerating ICG release. The findings of in vitro cellular uptake and cytotoxicity studies further demonstrated that the PEGylated ICG-carrying hybrid nanoparticles were efficiently internalized by MCF-7 cells compared to free ICG and realized intracellular acid-triggered rapid ICG liberation, thus enhancing anticancer effect of ICG-mediated PTT to potently kill cancer cells.

1. Introduction

Recently, photothermal therapy (PTT) has emerged as a favorable methodology for cancer treatment based on its minimal invasiveness, low systemic adverse effect, the remote spatiotemporal control, high specificity and therapeutic efficacy [1–5]. Near infrared (NIR) light with low absorption and scattering in biological tissues as well as deep tissue penetration has been considered to be the ideal optical source utilized in PTT [5–7]. To promote efficacy of photothermal tumor ablation, a varied of photosensitizers such as gold nanoparticles [8,9], carbon nanomaterials [10,11] and organic molecules [2,5–7] that strongly absorb NIR light to generate hyperthermia, have been extensively developed. Nevertheless, due to non-biodegradability and potential long-term toxicity of the aforementioned inorganic photosensitizers, their clinical applications still face serious challenges. In order to realize clinical use of PTT in tumor treatment, the NIR-absorbing organic photosensitizers have received considerable attention in the decade. Among them, indocyanine green (ICG), an amphiphilic tricarbocyanine dye, is approved by US Food and Drug Administration (FDA) for clinical applications of medical diagnosis and imaging [2,7,12]. Also, several studies reported that ICG showed promising potential in application of PTT owing to its NIR-triggered photothermal conversion capability [2,7,13,14]. However, the practical clinical use of ICG in PTT-mediated tumor treatment is largely limited by its some drawbacks including concentration-dependent aggregation, poor light and heat resistance, rapid degradation in polar solvent, high plasma protein binding ratio, lack of tumor targeting and short half-life in the body [2,7,13].

To conquer the disadvantages of ICG, over the past decade, various vehicles such as inorganic nanoparticles [15,16], liposomes [6,7], nanoemulsions [17], polymeric micelles and nanoparticles [18–22] have been increasingly designed for tumor-targeted ICG delivery. For example, Park's group designed a zwitterion fluorescent carbon dot (CD)-encapsulating mesoporous silica nanoparticle (MSN) to deliver ICG [16]. Through the hydrophobic and electrostatic interactions between zwitterion CDs and ICG molecules, ICG was encapsulated into MSN(CD). Under acidic condition, the ICG-MSN(CD) not only exhibited the

* Corresponding author.
E-mail address: whchiang@dragon.nchu.edu.tw (W.-H. Chiang).

https://doi.org/10.1016/j.colsurfb.2021.112048
Received 19 December 2020; Received in revised form 6 July 2021; Accepted 14 August 2021
Available online 16 August 2021

enhanced fluorescence signals and accelerated ICG release but also effectively killed MDA-MB-231 cells upon NIR-triggered hyperthermia. Moreover, as reported by Chen et al. [22], a robust, biocompatible, and dual-stimuli responsive ICG-loaded silk fibroin (SF) (ICG-SF) nanoparticles were fabricated by supercritical fluid technology. The results of in vitro and in vivo studies showed that the ICG-SF nanoparticles displayed acid-triggered ICG release to enhance accumulation of ICG close to the nuclei, thus potently suppressing tumor growth by NIR-activated PTT. On the other hand, to achieve fluorescence imaging-guided tumor PTT, Li and coworkers designed the ultra-pH-sensitive poly(ethylene glycol) (PEG)-b-(PR-r-ICG) nanomicelles capable of showing high tumor-to-normal tissue fluorescence contrast upon acid-triggered disintegration of micelles [2]. In comparison with free ICG, these ICG-conjugated nanomicelles exhibited longer blood circulation time and superior tumor accumulation, thereby significantly inhibiting tumor growth in A549 xenograft model via imaging-guided PTT.

To enhance anticancer effect of ICG-mediated PTT by promoting aqueous photo-stability and intracellular delivery of ICG, the hybrid polymeric nanoparticles equipped with acid-responsive detachable PEG surface coating employed as carriers of ICG were developed in this work. First, the amphiphilic polymer composed of methoxy-PEG (mPEG) and 1-octadecanamine (C18) with an acid-labile benzoic-imine bond was synthesized by Schiff base reaction (Scheme 1a) and characterized by Fourier transform infrared (FT-IR) and proton nuclear magnetic resonance (^{1}H-NMR). Through the hydrophobic anchoring of long-alkyl chains, the amphiphilic mPEG-benzoic-imine-C18 (mPEG-b-C18) and tocopheryl polyethylene glycol succinate (TPGS) segments were inserted on the surfaces of ICG-containing poly(lactic-co-glycolic acid) (PLGA) cores (Scheme 1b). The structural characteristics of ICG-loaded hybrid nanoparticles were explored by variable angle dynamic light scattering (DLS) technique, transmission electron microscopy (TEM) and zeta potential measurements. In addition to the optical and colloidal stability of ICG-loaded nanoparticles in aqueous phase, the in vitro ICG release performance in response to pH change was evaluated. Furthermore, the in vitro cellular uptake of ICG-loaded nanoparticles by MCF-7 cells and their NIR-triggered cytotoxicity were further studied.

2. Experimental section

2.1. Materials

ICG (95.4 %) was purchased from Chem-Impex (USA). Polyethylene glycol monomethylether (mPEG, M.W. = 2.0 kDa, 98 %), N,N′-dicyclohexylcarbodiimide (DCC, 99 %), 3-(4,5-Dimethylthiazol-2-yl)-2,5-diphenyltetrazolium bromide (MTT), 1-octadecanamine and pyrene (98 %) were acquired from Alfa Aesar (USA). *p*-formylbenzoic acid (95 %), N-hydroxysuccinimide (NHS, 98 %), 4-dimethylaminopyridine (DMAP, 98 %), D_2O (99.9 atom % D) and TPGS were purchased from Sigma-Aldrich (USA). Dulbecco's modified Eagle medium (DMEM), Hoechst 33,342, and fetal bovine serum (FBS) were purchased from Invitrogen (USA). Deionized water was produced from Milli-Q Synthesis (18 MΩ, Millipore). All other chemicals were reagent grade and used as received. MCF-7 cells (human breast cancer cell line) were obtained from Food Industry Research and Development Institute (Hsinchu City, Taiwan).

2.2. Synthesis of mPEG-b-C18 and mPEG-C18 adducts

The synthesis of mPEG-b-C18 based on Schiff base reaction of mPEG−CHO and 1-octadecanamine was conducted according to the protocol reported by Yang's group [23]. First, the mPEG−CHO utilized in this study was synthesized by the DCC/DMAP-mediated esterification of mPEG with *p*-formylbenzoic acid based on our previous approach [12]. The detailed synthetic process of mPEG−CHO is shown in Supporting Information. To obtain the mPEG-b-C18, mPEG−CHO (500 mg,

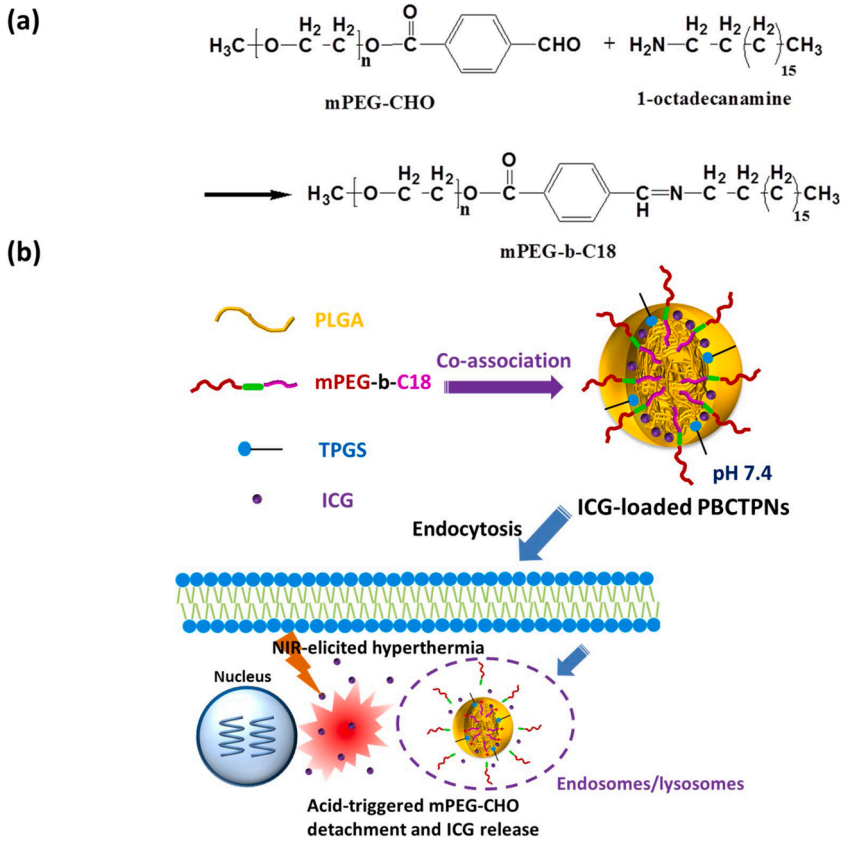

Scheme 1. (a) Synthetic route of the mPEG-b-C18 adducts. (b) Illustration of ICG-loaded PBCTPNs with acid-triggered mPEG−CHO detachment and rapid ICG liberation for cancer PTT.

1 equiv), 1-octadecanamine (80 mg, 1.2 equiv) and DMAP (61 mg, 2 equiv) were dissolved in dichloromethane (5.0 mL). The solution was stirred at room temperature for 36 h, following by removal of dichloromethane under reduced pressure. Subsequently, the product was dissolved in DMSO and dialyzed (Cellu Sep MWCO 1000) against pH 8.0 deionized water at 4 °C to remove DMSO. The product was collected by freeze-drying. The synthetic procedure of mPEG-b-C18 was presented in Scheme 1a. For comparison, the mPEG-C18 without benzoic-imine bond was synthesized by esterification of mPEG with stearic acid (Scheme S1). mPEG (1 g, 1 equiv), stearic acid (0.29 g, 2 equiv), DCC (0.206 g, 2 equiv) and DMAP (0.012 g, 0.2 equiv) were dissolved in dichloromethane (5.0 mL). The reaction was carried out under stirring at 25 °C for 24 h. After removal of dicyclohexylcarbodiurea by filtration, the solution was concentrated under reduced pressure. The product was then collected by precipitation from cold diethyl ether and dried under vacuum overnight.

2.3. Characterization of mPEG-b-C18 and mPEG-C18

FT-IR spectra of mPEG-b-C18 and mPEG-C18 were attained using a HORIBA FT-720 FT-IR spectrometer. The dried sample was pressed with KBr under vacuum and scanned from 4000 to 400 cm^{-1}. The compositions of mPEG-b-C18 and mPEG-C18 were determined by ^{1}H-NMR spectroscopy (Agilent DD2 600 MHz NMR spectrometer) using $CDCl_3$ as the solvent. Also the UV/Vis spectra of mPEG-b-C18 and mPEG-C18 in DMSO were attained using a Hitachi U2900 UV/Vis spectrophotometer. The fluorescence spectra of pyrene in aqueous solutions of mPEG-b-C18 and mPEG-C18 assemblies at pH 7.4 and 5.5, respectively, were obtained with a Hitachi F-2700 fluorescence spectrometer. The emission spectra were recorded in the range from 350 to 500 nm based on the excitation wavelength of 336 nm.

2.4. Preparation of ICG-loaded PLGA-based nanoparticles

The ICG-loaded PLGA-based nanoparticles coated with TPGS combined with either mPEG-b-C18 or mPEG-C18 adducts were fabricated by the one-step nanoprecipitation method. The mPEG-b-C18/TPGS/PLGA nanoparticles (denoted hereinafter as PBCTPNs) laden with ICG were prepared as follows. PLGA (2.0 mg), mPEG-b-C18 (1.0 mg), TPGS (0.1 mg) and ICG (0.2 mg) dissolved in DMSO (0.25 mL) were added dropwise into the pH 8.0 phosphate buffer (1.75 mL) under stirring. The solution was then stirred at room temperature for 30 min, following by equilibrium of additional 30 min. Subsequently, the ICG-loaded PBCTPN solution was dialyzed (Cellu Sep MWCO 12000–14000) against pH 8.0 phosphate buffer at 4 °C for 24 h to eliminate DMSO and un-loaded ICG. For comparison, PLGA nanoparticles (PNs) and mPEG-C18/TPGS/PLGA nanoparticles (PCTPNs) loaded with ICG were prepared in a similar way.

2.5. Characterization of various ICG-loaded nanoparticles

The mean hydrodynamic particle diameter (D_h) and size distribution of various ICG-loaded nanoparticles in aqueous solutions were determined using a Brookhaven BI-200SM goniometer equipped with a BI-9000 AT digital correlator using a solid-state laser (35 mW, $\lambda = 637$ nm) detected at a scattering angle of 90 °. The data presented herein represent an average of at least triplicate measurements. Also, to gain insight into the morphology of ICG-loaded PBCTPNs and PCTPNs in aqueous solution of pH 7.4, the angular dependence of their autocorrelation functions was assessed by the above instrument. The zeta potential of various ICG-carrying nanoparticles in aqueous solutions of different pH was measured by a Nanobrook 90Plus PALS (Brookhaven, USA). The TEM images of ICG-loaded nanoparticles negatively stained with uranyl acetate were obtained from a JEOL JEM-1400 CXII microscope. The absorption spectra of free ICG and ICG-containing nanoparticles in aqueous solutions at different time intervals were obtained by a Hitachi U2900 UV/Vis spectrophotometer.

For quantitation of ICG entrapped within nanoparticles, a prescribed volume of the purified ICG-loaded nanoparticle solution was lyophilized and then dissolved into DMSO to disrupt colloidal structure. The absorbance of ICG at 794 nm was determined by a Hitachi U2900 UV/Vis spectrophotometer. Drug loading efficiency (DLE) and drug loading content (DLC) were estimated by the following equations

DLE (%) = (weight of loaded ICG/weight of ICG in feed) × 100 %.

DLC (%) = (weight of loaded ICG/total weight of the ICG-loaded nanoparticles) × 100 %.

2.6. In vitro ICG release profiles

In ICG release study, the dialysis (Cellu Sep MWCO 12,000~14,000) of the ICG-loaded nanoparticle solutions (3.0 mL) with phosphate buffered saline (PBS, pH 7.4) and acetate buffer (pH 5.5) (40 mL), respectively, was conducted at 37 °C. The internal sample was taken out periodically for measurement of maximum ICG absorbance. The sample solution was put back into the dialysis tube after each measurement. The cumulative ICG release (%) was obtained by the formula:

Cumulative ICG release (%) = ((Initial ICG absorbance - ICG absorbance at different time points)/initial ICG absorbance) × 100 %.

2.7. Temperature measurement under NIR laser irradiation

Various ICG-carrying nanoparticles and free ICG in PBS (1.0 mL) were irradiated with 808 nm NIR laser (1.0 W/cm^2) for 5 min. The solution temperature was monitored during NIR irradiation by an infrared thermal imaging camera (Thermo Shot F20, NEC Avio Infrared, Germany).

2.8. In vitro cellular uptake

MCF-7 cells (2×10^5 cells/well) were seeded in 6-well plate containing 22 mm round glass coverslips and cultured overnight. The cells were then incubated with free ICG, ICG-loaded PN, PCTPNs and PBCTPNs, respectively, at an ICG concentration of 20 μM for 4 h. After being washed twice with PBS and fixed with 4 % formaldehyde, the cells were stained with Hoechst 33,342 for 15 min, and the slides were rinsed three times with PBS. The cellular uptake was observed by confocal laser scanning microscopy (CLSM) (Olympus, FluoView FV3000, Japan) at the excitation wavelengths of 405 and 633 nm for Hoechst and ICG, respectively.

2.9. In vitro photothermal effects

MCF-7 cells (1×10^5 cells/well) seeded in a 24-well plate were incubated in DMEM containing 10 % FBS and 1% penicillin at 37 °C for 24 h. The medium was then replaced with 1.0 mL of fresh DMEM containing either free ICG or various ICG-carrying nanoformulations (ICG concnetration = 15 μM), following by 24 h incubation. Subsequently, cells were washed twice with PBS and detached with trypsine-EDTA. The cell pellets collected by centrifugation were dispersed in DMEM (100 μL) and then exposed to irradiation of a 808 nm NIR laser (1.0 W/cm^2) for 5 min. The laser-treated cells (1×10^4 cells/well) were reseeded in a 96-well plate and incubated for 24 h. The cell viability was examined by MTT assay and the absorbance of the resulting solution was measured at 570 nm using a BioTek 800TS microplate reader. The viability of MCF-7 cells receiving various nanoformulations without NIR laser irradiation was assessed in a similar manner.

3. Results and discussion

3.1. Synthesis and characterization of mPEG-b-C18 and mPEG-C18

The mPEG−CHO used in this work was attained by the conjugation of mPEG with *p*-formylbenzoic acid as reported in our previous work [12]. As presented in the FT-IR spectra (Fig. 1a and b), in addition to the characteristic absorption bands at 1108 and 2885 cm^{-1} for CO and CH—— stretching vibration of mPEG, the absorption bands at 1644 and 1709 cm^{-1} for C═O stretching vibration of aldehyde and ester groups, respectively, and at 1568 and 1541 cm^{-1} for C═C stretching vibration of benzene ring from mPEG−CHO were observed. Also, compared to the ^{1}H-NMR spectrum of mPEG (Fig. 2a), the appearance of feature proton signals of benzene ring at δ 8.1 and 8.3 ppm, and of aldehyde group at δ 10.1 ppm were attained in the ^{1}H-NMR spectrum of mPEG−CHO (Fig. 2b), demonstrating the successful coupling of mPEG and *p*-formylbenzoic acid. According to the signal integral ratio of the methoxy protons (δ 3.4 ppm) and aldehyde proton (δ 10.1 ppm) of mPEG−CHO, the conjugation efficiency was estimated to be ca. 95 %. Upon the formation of benzoic-imine bond from Schiff base reaction between aldehyde and primary amine of mPEG−CHO and 1-octadecanamine, respectively, the mPEG-b-C18 was acquired. In the FT-IR spectrum of mPEG-b-C18 (Fig. 1d), the presence of a new absorption peak at 1649 cm^{-1} from CN stretching vibration indicates the effective conjugation of mPEG═−CHO and 1-octadecanamine. Furthermore, as revealed in the ^{1}H-NMR spectrum of mPEG-b-C18 (Fig. 2c), the complete disappearance of the proton signals of aldehyde group at δ 10.1 ppm and the presence of proton signals of aliphatic alkyl group at δ 0.8~1.8 ppm, and of benzoic-imine group at δ 8.5 ppm strongly verify the fruitful conjugation of mPEG−CHO and 1-octadecanamine. Based on the signal integral ratio of the methyl and imine protons of mPEG-b-C18, the conjugation efficiency was obtained to be ca. 98 %. To confirm whether the benzoic-imine linker of mPEG-b-C18 under acidic condition could be hydrolysed, the mPEG-b-C18 was pre-treated with aqueous solution of pH 5.0 for 12 h and characterized by ^{1}H-NMR. As shown in Fig. 2e, the appearance of the proton signal of aldehyde group at δ 10.1 ppm and the disappearance of proton signal of imine group at δ 8.5 ppm clearly illustrate the acid-elicited cleavage of benzoic-imine bond of mPEG-b-C18.

For comparison, the mPEG-C18 without benzoic-imine bond was prepared by the DCC/DMAP-mediated esterification of mPEG with stearic acid. In the ^{1}H-NMR spectrum of mPEG-C18 (Fig. 2d), based on the integration ratio of the signals from methoxy protons (δ 3.4 ppm) of mPEG and the tail methyl protons (δ 0.82 ppm) of stearic acid, the coupling efficiency was assessed to be ca. 95 %. Distinct from mPEG-C18, the mPEG-b-C18 exhibited the feature absorption peak of benzene ring at 260 nm due to the presence of benzoic-imine bonds (Fig. S1). Based on the coupling of the hydrophilic mPEG with hydrophobic long alkyl chain (C18), the obtained amphiphilic mPEG-b-C18 and mPEG-C18 adducts were expected to self-assemble into polymeric assemblies in aqueous solution. Notably, the I_3/I_1 value (ca. 1.05) of pyrene in mPEG-b-C18-containing aqueous solution of pH 7.4 is significantly higher than that (ca. 0.74) of pyrene in mPEG-C18 suspension at the same pH (Fig. S2), revealing that the mPEG-b-C18 adducts tend to self-associate into more hydrophobic assemblies upon π-π stacking of the benzoic-imine groups combined with association of long alkyl chains. It should be noted that the I_3/I_1 value of pyrene in mPEG-b-C18 dispersion was appreciably decreased from 1.05 to 0.87 with the solution pH being lowered from 7.4–5.5. This implies that the hydrophobicity of mPEG-b-C18-consistituated assemblies was reduced due to the acid-triggered detachment of mPEG−CHO from assemblies via acid-activated hydrolysis of benzoic-imine linkages. By contrast, due to the lack of pH-responsive linkers, no significant variation in the I_3/I_1 value of pyrene in mPEG-C18-containing solution was observed with the same pH stimulus.

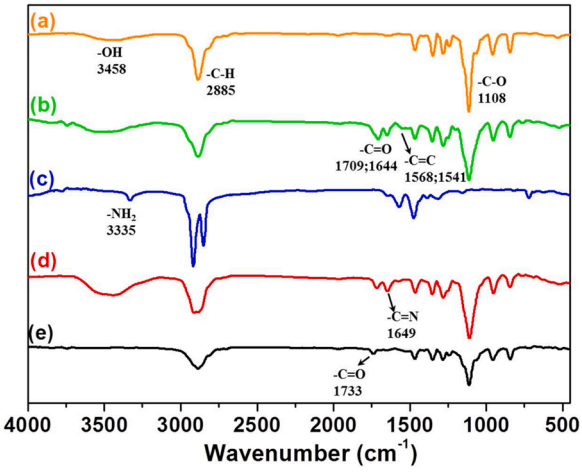

Fig. 1. FT-IR spectra of (a) mPEG, (b) mPEG−CHO, (c) n-octadecane amine, (d) mPEG-b-C18 and (e) mPEG-C18.

3.2. Preparation and characterization of ICG-carrying PLGA-based nanoparticles

In our previous work [24], it was demonstrated that the amphiphilic ICG molecules were hydrophobically attached on the surfaces of PLGA/TPGS-constituted nanoparticles. In this study, in order to achieve effective intracellular ICG release, the ICG-loaded PBCTPNs were attained by the hydrophobic anchor of the amphiphilic pH-responsive mPEG-b-C18 adducts and TPGS segments on the surfaces of ICG-carrying PLGA cores. For comparison, the ICG-loaded PCTPNs with surface coating of non-pH-sensitive mPEG-C18 and TPGS, and ICG-loaded PNs without surface coating were also fabricated. As shown in Table 1 and Fig. 3a, the mean hydrodynamic diameter (D_h) of the ICG-loaded PBCTPNs and PCTPNs in PBS was somewhat larger than that of ICG-loaded PNs due to the presence of the additional coating layer [25,26]. Importantly, the surface coating of ICG-loaded PBCTPNs and PCTPNs significantly promoted ICG loading efficiency (Table 1), being probably ascribed to the enhanced hydrophobic association of long alkyl chain of mPEG-b-C18 or mPEG-C18 with ICG. Moreover, for ICG-loaded PBCTPNs and PCTPNs, the relaxation frequency (Γ) and the square of the scattering vector (q^2) presented a high linear relationship as revealed in the variable angle DLS data (Fig. 3b and c), suggesting that these nanoparticles in aqueous solution had a spherical shape [12,18]. Also, the well-dispersed spherical shape of ICG-loaded PBCTPNs and PCTPNs was observed in their TEM images (Fig. 3d and e). Notably, the results of DLS and TEM showed the larger particle size of ICG-loaded PBCTPNs relative to that of ICG-loaded PCTPNs (Table 1, Fig. 3a, d and e). Presumably, the extensive π-π stacking and hydrophobic interaction of benzene ring-containing mPEG-b-C18 adducts with ICG molecules were apt to form thick coating layer on the surfaces of PLGA cores (Scheme 1). On the other hand, it should be mentioned that the particle sizes of ICG-loaded nanoparticles observed by TEM were appreciably smaller than those determined by DLS due to the dehydration of nanoparticles during TEM study.

Compared to free ICG, the ICG-loaded PNs, PBCTPNs and PCTPNs exhibited appreciable red shift of characteristic ICG absorption peak from 776 to 797 nm (Fig. 4a), being as a result of the attachment of ICG molecules to the PLGA cores. Similar findings have also been mentioned elsewhere [19,24]. Notably, a minor decrease in the normalized absorbance of ICG-loaded nanoparticles in PBS over 7 days was attained while the absorbance of free ICG was remarkably declined (Figs. 4b and S3). Also, different from enormous precipitation of free ICG in PBS, the ICG-loaded nanoparticles effectively prevented ICG from self-aggregation (the inset of Fig. 4b), thus promoting aqueous photostability of ICG molecules. Furthermore, the ICG-carrying nanoparticles

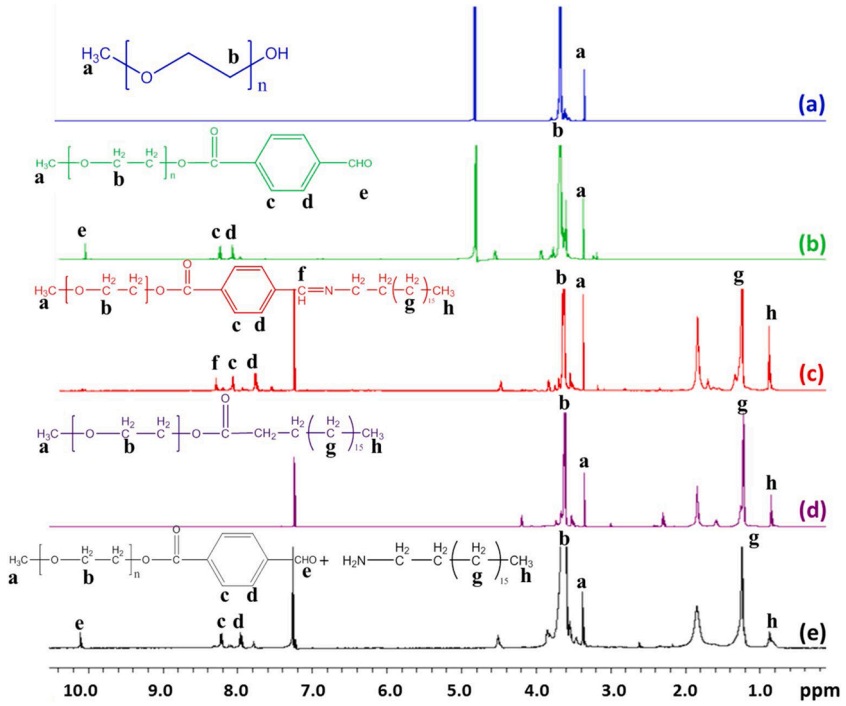

Fig. 2. ^{1}H-NMR spectra of (a) mPEG and (b) mPEG−CHO in D_2O, (c) mPEG-b-C18, (d) mPEG-C18 and (e) acid-treated mPEG-b-C18 in $CDCl_3$.

Table 1
DLS data, drug loading efficiency and content of ICG-loaded nanoparticles.

Sample	D_h (nm)	PDI	DLE (%)	DLC (wt %)
ICG-loaded PNs	120 ± 15	0.20 ± 0.04	52.2 ± 3.6	5.23 ± 0.1
ICG-loaded PCTPNs	138 ± 5	0.23 ± 0.03	70.7 ± 4.9	4.26 ± 0.2
ICG-loaded PBCTPNs	159 ± 8	0.25 ± 0.01	74.4 ± 3.2	4.51 ± 0.1

remained essentially unchanged particle size in PBS at 37 °C over a time period of 14 days (Fig. 4c) and in 10 % FBS-containing PBS within 12 h (Fig. 4d). Based on these findings, it is anticipated that the ICG-loaded nanoparticles could maintain stable colloidal structure under physiological conditions.

3.3. pH-triggered mPEG−CHO detachment and in vitro ICG release

Notably, in aqueous solution of pH 7.4, the zeta potential of ICG-loaded PBCTPNs and PCTPNs was appreciably lower compared to that of ICG-loaded PNs (Fig. 5a), indicating that the mPEG-rich surface coating of the former could partly shield the negative charges of ICG molecules inserting on PLGA cores. Similar results regarding the sheltering of surface charges of various functionalized nanoparticles by their PEG-constituted shells have been also presented elsewhere [23,25,27,28]. Furthermore, it should be noted that the zeta potential (-19.6 mV) of ICG-loaded PBCTPNs at pH 7.4 was somewhat higher than that (-12.0 mV) of ICG-loaded PCTPNs. It was assumed that some of ICG molecules were encapsulated within the coating layer of PBCTPNs upon their π-π

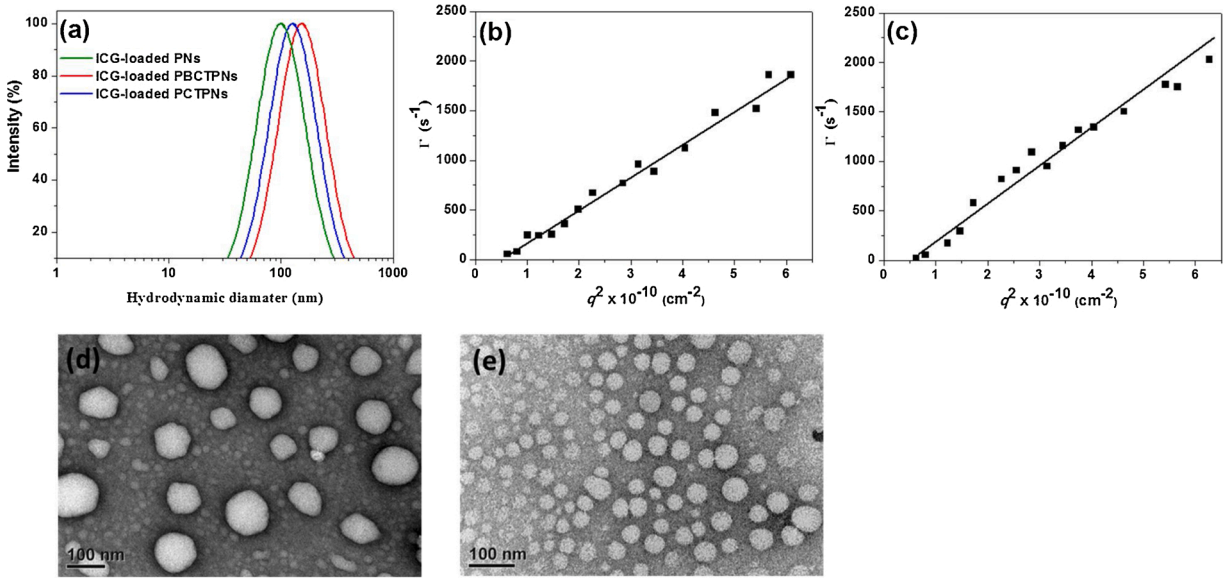

Fig. 3. (a) DLS size distribution profiles of various ICG-loaded nanoparticles in pH 7.4 PBS. Angle-dependent correlation ofΓversus q^2 of (b) ICG-loaded PBCTPNs and (c) ICG-loaded PCTPNs in PBS. TEM images of (d) ICG-loaded PBCTPNs and (e) ICG-loaded PCTPNs.

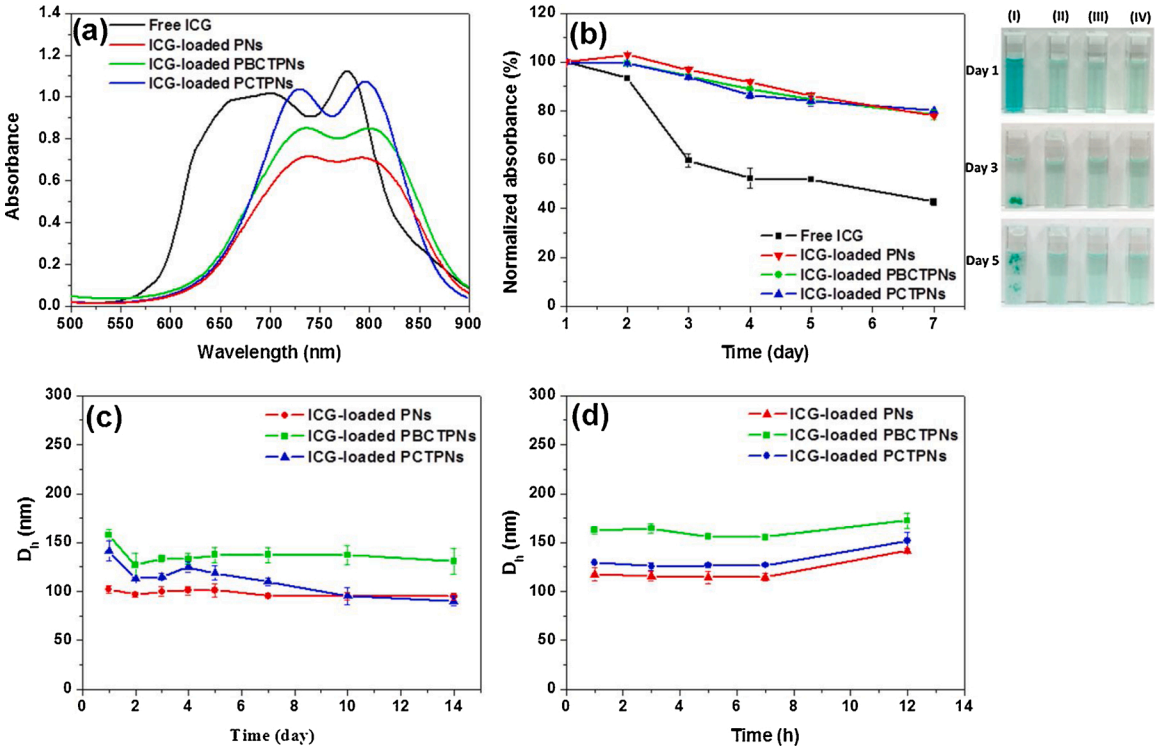

Fig. 4. (a) UV/Vis spectra of free ICG and ICG-loaded PNs, PBCTPNs and PCTPNs in pH 7.4 PBS. (b) Normalized maximum absorbance and photographs of (i) free ICG and (ii) ICG-loaded PNs, (iii) ICG-loaded PBCTPNs and (iv) ICG-loaded PCTPNs in PBS at 37 °C. Mean hydrodynamic diameters (D_h) of various ICG-loaded nanoparticles in (c) PBS and (d) 10 % FBS-containing PBS at different time intervals.

stacking and hydrophobic interaction with benzene ring-containing mPEG-b-C18 adducts, thus leading to the reduced shielding of negative charges by outer mPEG segments. By contrast, for ICG-loaded PCTPNs, because most of ICG molecules inclined to hydrophobically attach on the surfaces of PLGA cores in the lack of benzene ring in mPEG-C18, the outside mPEG segments could sufficiently shield the negative charges of ICG molecules. With the solution pH being adjusted from pH 7.4–5.5, different from the nearly unvaried zeta potentials of ICG-loaded PNs and PCTPNs, the zeta potential of ICG-loaded PBCTPNs was considerably changed from negative to slightly positive value. Such an acid-elicited variation in zeta potential of ICG-loaded PBCTPNs strongly demonstrates that the mPEG−CHO segments can be segregated from ICG-loaded PBCTPNs upon hydrolysis of benzoic-imine linkers of mPEG-b-C18 adducts, thus enabling exposure of the positive charges of protonated 1-octadecanamine (Scheme 1). In comparison, due to the absence of acid-labile linkages in mPEG-C18 adducts, the mPEG segments cannot be detached from the ICG-carrying PCTPNs in response to pH reduction, thereby resulting in no significant change in the zeta potential. On the other hand, the ICG-loaded PBCTPNs maintained virtually unchanged particle size in the solution pH range 5.5∼7.4 (Fig. S4), illustrating that the mPEG−CHO detachment of ICG-loaded PBCTPNs could not affect their aqueous colloidal stability.

In order to explore the effect of PEG−CHO shedding on payload release of ICG-loaded PBCTPNs, the in vitro ICG dissolution was performed by dialysis method. Fig. 5b showed that, in comparison with relatively quick diffusion of free ICG molecules (ca. 70 %) through the dialysis tube at pH 7.4 over a period of 7 h, the cumulative ICG release of ICG-loaded nanoparticles at the same pH were prominently reduced. This suggests that the hydrophobic PLGA matrix as physical barrier could hinder leakage of ICG molecules to some degree. Notably, with pH reduction from 7.4–5.5, the ICG-loaded PBCTPNs displayed a remarkably increased cumulative ICG release (> 65 % over 24 h) compared to ICG-loaded PNs and PCTPNs (Fig. 5c). This indicates that the release of ICG entrapped within benzene ring-rich coating layers of ICG-loaded PBCTPNs could be accelerated via the lowered π-π stacking and hydrophobic interactions between ICG molecules and PBCTPNs driven by acid-activated mPEG−CHO detachment. Similarly, as reported by Tian group, through acid-induced PEG layer detachment of the paclitaxel/curcumin-loaded pH multistage responsive micelles, the drug release rate was appreciably accelerated [28].

3.4. *In vitro NIR-triggered hyperthermia*

Based on the inherent photothermal conversion capability of ICG, the hyperthermia effect of various ICG-loaded nanoparticles in aqueous solutions exposed to NIR laser irradiation of 808 nm was assessed by monitoring the solution temperature with an infrared thermal imaging camera. During NIR laser irradiation, the temperatures of free ICG and ICG-carrying nanoparticle solutions were considerably elevated through the ICG-mediated photothermal effect (Fig. 5d), whereas no significant change in temperature of PBS was attained (data not shown). Notably, at the same irradiation time, the temperature of ICG-loaded nanoparticle solutions was apparently raised compared with that of free ICG solution. This could be ascribed to that the absorption of ICG attached on the surfaces of PLGA nanoparticles undergo remarkable red-shift (from 776 to 797 nm) to match the central wavelength (808 nm) of the diode laser employed, thus promoting the photo-thermal conversion capability [18,24]. Also, the similar profiles of temperature variation for aqueous solutions of different ICG-loaded nanoparticles under NIR laser irradiation clearly illustrate that the NIR-triggered hyperthermia ability of ICG-loaded nanoparticles could not be affected by the surface coatings. Moreover, when the ICG concentration was increased from 15 to 25 μM, the temperature of ICG-loaded PBCTPN solution under NIR laser irradiation could be further elevated over 50 °C (Fig. S5). In general, high temperature beyond 50 °C is required to generate effective potency of cancer thermotherapy [2,3,24]. As expected, the NIR-triggered hyperthermia of ICG-loaded PBCTPNs was also boosted by enhancing laser power density (Fig. S6).

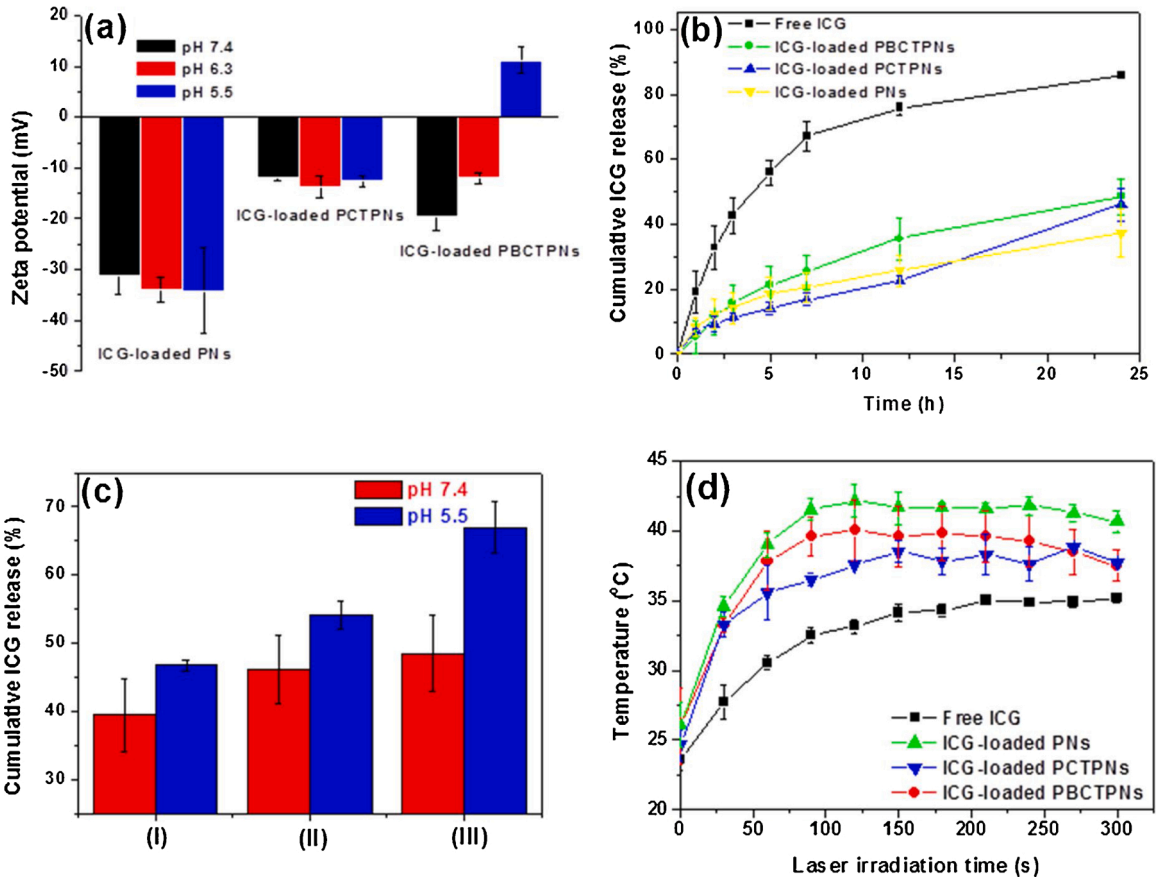

Fig. 5. (a) Zeta potential of ICG-loaded nanoparticles in aqueous solutions of different pH. (b) Cumulative ICG release profiles of various ICG-loaded nanoparticles in PBS. (c) Cumulative ICG release of ICG-loaded PNs (i), PCTPNs (ii) and PBCTPNs (iii) in aqueous solutions of pH 7.4 and 5.5 for 24 h. (d) Temperature profiles of free ICG and various ICG-loaded nanoparticles in PBS (ICG concentration = 15 μM) under irradiation of 808 nm NIR laser (1.0 W/cm^2).

3.5. *In vitro cellular uptake and PTT efficacy*

The cellular uptake of ICG-loaded PBCTPNs by MCF-7 cells was observed by CLSM. As shown in Fig. 6a, the ICG fluorescence was remarkably found in the cytoplasm of MCF-7 cells treated with ICG-loaded PBCTPNs and PCTPNs in comparison with that of cells incubated with free ICG and ICG-loaded PNs, illustrating that the endocytosis of ICG-carrying nanoparticles with PEG-rich surface coating could be promoted compared to that of non-PEGylated ICG-loaded nanoparticles and free ICG molecules. The phenomenon could be ascribed to that the surface coating of ICG-loaded PBCTPNs and PCTPNs could partly shield the negative charges of ICG molecules (Fig. 5a), thus lowering repulsion force between the nanoparticles and negatively-charged cell membranes. By contrast, in the absence of PEGylation, the cellular uptake of the free ICG-based assemblies and non-PEGylated ICG-loaded PNs were largely hindered by their negative charges-rich surfaces. Furthermore, MCF-7 cells incubated with ICG-loaded PBCTPNs showed considerably higher ICG fluorescence intensity in the cytoplasm relative to the cells treated with ICG-carrying PCTPNs, suggesting that the endocytosed ICG-loaded PBCTPNs within acidic endosomes and lysosomes could accelerate liberation of ICG molecules by the acid-elicited mPEG−CHO detachment.

The anticancer activity of NIR-triggered hyperthermia on MCF-7 cells treated with free ICG or ICG-carrying nanoparticles was further evaluated. As presented in Fig. 6b, in the lack of NIR laser irradiation, the quite high viability (over 85 %) of MCF-7 cells receiving either free ICG or ICG-loaded nanoparticles (ICG concentration = 15 μM) was attained, revealing the nontoxicity of ICG molecules and the drug-free nanocarriers to MCF-7 cells. Upon 5 min NIR laser radiation, the viability of the treated MCF-7 cells was remarkably reduced, signifying the hyperthermia-induced cell death. It should be noted that the ICG-carrying PBCTPNs maximized the anticancer efficacy of ICG-mediated PTT relative to other test groups. The results could be attributed to the following two reasons: First, the PEGylated ICG-loaded PBCTPNs were efficiently internalized by MCF-7 cells, thus significantly facilitating intracellular ICG delivery. Second, the internalized ICG-loaded PBCTPNs within acidic organelles could accelerate ICG liberation by the acid-triggered mPEG−CHO dissociation, thus aiding accumulation of ICG close to nuclei to boost its PTT-mediated anticancer potency [22]. Based on these findings, it can be concluded that the ICG-loaded PBCTPNs designed in this work are greatly promising for cancer PTT.

4. Conclusions

In order to achieve intracellular ICG delivery for improved PTT-meditated anticancer efficacy, the hybrid nanoparticles composed of hydrophobic PLGA cores and mPEG-b-C18/TPGS surface coating were designed as vehicles of ICG. The angle-dependent DLS and TEM studies revealed that the ICG-loaded PBCTPNs had a well-dispersed spherical shape. Moreover, the ICG-loaded PBCTPNs in PBS maintained outstanding colloidal stability and effectively inhibited ICG self-aggregation and leakage, thereby increasing aqueous photostability of ICG molecules. Notably, with solution pH adjusted from pH 7.4–5.5, the detachment of mPEG−CHO segments from ICG-carrying PBCTPNs upon acid-triggered hydrolysis of benzoic-imine linkers within mPEG-b-C18 considerably promoted ICG release. Under NIR laser irradiation, the ICG-loaded PBCTPNs displayed satisfied capability of generating hyperthermia. In vitro cellular uptake findings indicate that the

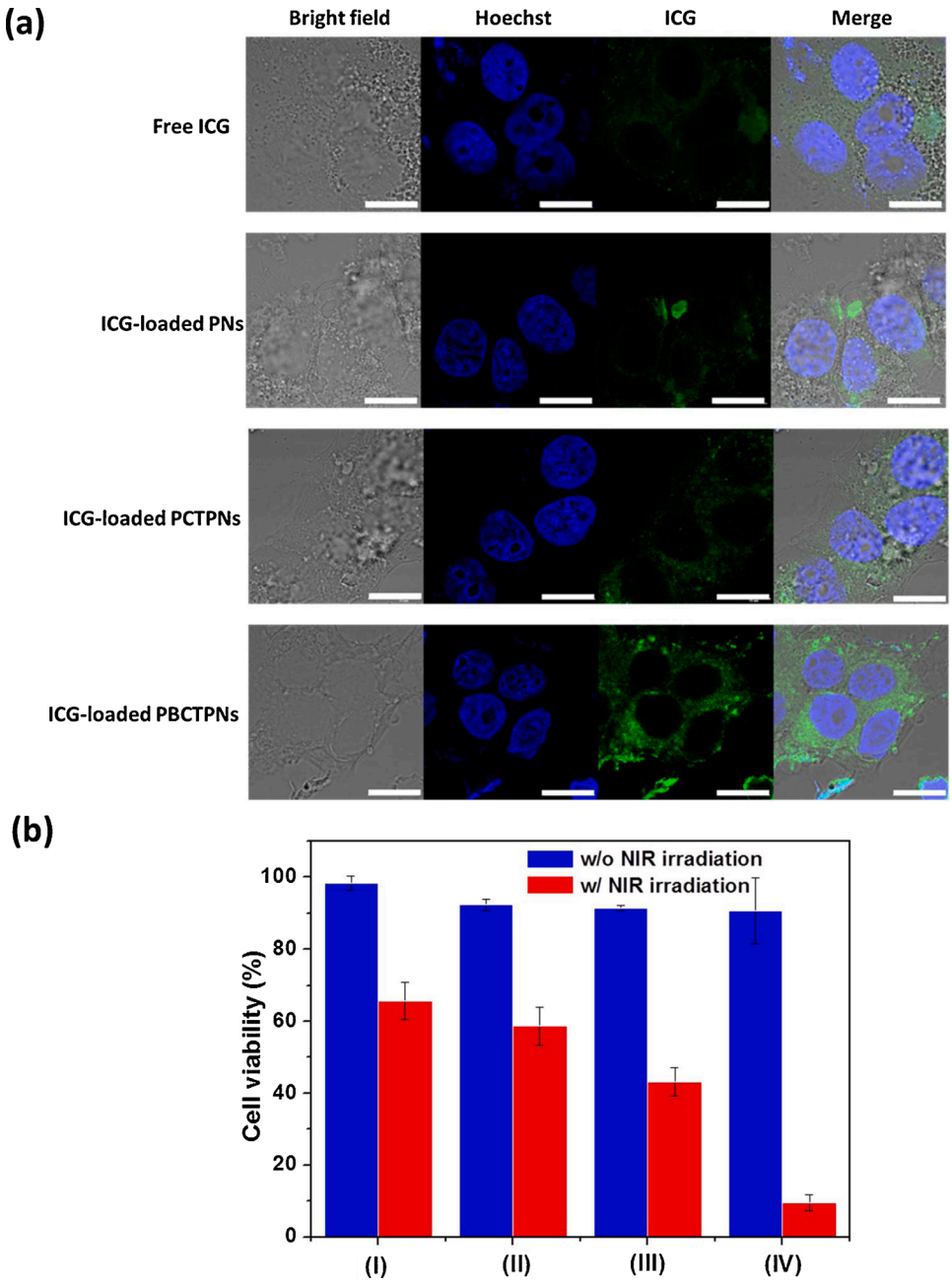

Fig. 6. (a) CLSM images of MCF-7 cells incubated with free ICG, ICG-loaded PNs, PCTPNs and PBCTPNs (ICG concentration = 20 μM) at 37 °C for 4 h. Scale bars are 15 μm. (b) Cell viability of MCF-7 cells incubated with (I) free ICG, (II) ICG-loaded PNs, (III) ICG-loaded PCTPNs and (IV) ICG-loaded PBCTPNs for 24 h with and without the 5-min NIR laser irradiation.

internalization of the PEGylated ICG-carrying PBCTPNs by MCF-7 cells can be enhanced. Through the acid-activated intracellular ICG release combined with NIR irradiation, the PTT delivered by ICG-loaded PBCTPNs prominently killed MCF-7 cells. Taken together, the acid-responsive ICG-loaded hybrid nanoparticles show great promising for boosting potency of the cancer PTT.

CRediT authorship contribution statement

Chih-Wei Ting: Conceptualization, Investigation, Resources, Methodology. **Ya-Hsuan Chou:** Investigation, Validation, Methodology. **Shih-Yu Huang:** Investigation, Resources. **Wen-Hsuan Chiang:** Conceptualization, Writing - review & editing, Supervision, Project administration, Funding acquisition.

Declaration of Competing Interest

The authors report no conflict of interest.

Acknowledgements

This work is supported by the Ministry of Science and Technology (MOST 107-2622-E-005-008 -CC3 and MOST 108-2221-E-005 -024 -MY2), Taiwan.

Appendix A. Supplementary data

Supplementary material related to this article can be found, in the online version, at doi:https://doi.org/10.1016/j.colsurfb.2021.112048.

References

[1] Q. Chen, L. Xu, C. Liang, C. Wang, R. Peng, Z. Liu, Photothermal therapy with immune-adjuvant nanoparticles together with checkpoint blockade for effective cancer immunotherapy, Nat. Commun. 7 (2016) 13193.

[2] Z. Li, Q. Yin, B. Chen, Z. Wang, Y. Yan, T. Qi, W. Chen, Q. Zhang, Y. Wang, Ultra-pH-sensitive indocyanine green-conjugated nanoprobes for fluorescence imaging-guided photothermal cancer therapy, Nanomedicine 17 (2019) 287–296.

[3] L. Zhu, P. Li, D. Gao, J. Liu, Y. Liu, C. Sun, M. Xu, X. Chen, Z. Sheng, R. Wang, Z. Yuan, L. Cai, Y. Ma, Q. Zhao, pH-sensitive loaded retinal/indocyanine green micelles as an "all-in-one" theranostic agent for multi-modal imaging in vivo guided cellular senescence-photothermal synergistic therapy, Chem. Commun. 55 (2019) 6209–6212.

[4] L. Luo, Y. Bian, Y. Liu, X. Zhang, M. Wang, S. Xing, L. Li, D. Gao, Combined near infrared photothermal therapy and chemotherapy using gold nanoshells coated liposomes to enhance antitumor effect, Small 12 (2016) 4103–4112.

[5] I.L. Lu, T.I. Liu, H.C. Lin, S.H. Chang, C.L. Lo, W.H. Chiang, H.C. Chiu, IR780-loaded zwitterionic polymeric nanoparticles with acidity-induced agglomeration for enhanced tumor retention, Eur. Polym. J. 122 (2020), 109400.

[6] L. Yu, A. Dong, R. Guo, M. Yang, L. Deng, J. Zhang, DOX/ICG coencapsulated liposome-coated thermosensitive nanogels for NIR-triggered simultaneous drug release and photothermal effect, ACS Biomater. Sci. Eng. 4 (2018) 2424–2434.

[7] H.J. Yoon, H.S. Lee, J.Y. Lim, J.H. Park, Liposomal indocyanine green for enhanced photothermal therapy, ACS Appl. Mater. Interfaces 9 (2017) 5683–5691.

[8] W. Yang, H. Liang, S. Ma, D. Wang, J. Huang, Gold nanoparticle based photothermal therapy: development and application for effective cancer treatment, SM&T 22 (2019) e00109.

[9] F. Zhao, X. Li, J. Li, Y. Dou, L. Wang, M. Wu, Y. Liu, J. Chang, X. Zhang, Activatable ultrasmall gold nanorods for "off–on" fluorescence imaging-guided photothermal therapy, J. Mater. Chem. B 5 (2017) 2145–2151.

[10] W. Liu, X. Zhang, L. Zhou, L. Shang, Z. Su, Reduced graphene oxide (rGO) hybridized hydrogel as a near-infrared(NIR)/pH dual-responsive platform for combined chemo-photothermal therapy, J. Colloid Inter. Sci. 536 (2019) 160–170.

[11] R. Lima-Sousa, D. de Melo-Diogo, C.G. Alves, E.C. Costa, P. Ferreira, R.O. Louro, I. J. Correia, Hyaluronic acid functionalized green reduced graphene oxide for targeted cancer photothermal therapy, Carbohydr. Polym. 200 (2018) 93–99.

[12] S.C. Liao, C.W. Ting, W.H. Chiang, Functionalized polymeric nanogels with pH-sensitive benzoic-imine cross-linkages designed as vehicles for indocyanine green delivery, J. Colloid Inter. Sci. 561 (2020) 11–22.

[13] R. Liu, J. Tang, Y. Xu, Y. Zhou, Z. Dai, Nano-sized indocyanine green J-aggregate as a one-component theranostic agent, Nanotheranostics 1 (2017) 430–439.

[14] C.C.L. Cheung, G. Ma, K. Karatasos, J. Seitsonen, J. Ruokolainen, C.R. Koffi, H.A.F. M. Hassan, W. Al-Jamal, Liposome-templated indocyanine green J-aggregates for in vivo near-infrared imaging and stable photothermal heating, Nanotheranostics 4 (2020) 91–106.

[15] T. Wang, S. Li, Z. Zou, L. Hai, X. Yang, X. Jia, A. Zhang, D. He, X. He, K. Wang, A zeolitic imidazolate framework-8-based indocyanine green theranostic agent for infrared fluorescence imaging and photothermal therapy, J. Mater. Chem. B 6 (2018) 3914–3921.

[16] B. Ryplida, G. Lee, I. In, S.Y. Park, Zwitterionic carbon dot-encapsulating pH-responsive mesoporous silica nanoparticles for NIR light-triggered photothermal therapy through pH-controllable release, Biomater. Sci. 7 (2019) 2600–2610.

[17] E.H. Lee, J.K. Kim, J.S. Lim, S.J. Lim, Enhancement of indocyanine green stability and cellular uptake by incorporating cationic lipid into indocyanine green-loaded nanoemulsions, Colloids Surf. B 136 (2015) 305–331.

[18] C.W. Hsu, M.H. Hsieh, M.C. Xiao, Y.H. Chou, T.H. Wang, W.H. Chiang, pH-responsive polymeric micelles self-assembled from benzoic-imine-containing alkyl-modified PEGylated chitosan for delivery of amphiphilic drugs, Int. J. Biol. Macromol. 163 (2020) 1106–1116.

[19] K.T. Hou, T.I. Liu, H.C. Chiu, W.H. Chiang, DOX/ICG-carrying γ-PGA-g-PLGA-based polymeric nanoassemblies for acidtriggered rapid DOX release combined with NIR-activated photothermal effect, Eur. Polym. J. 110 (2019) 283–292.

[20] P.R. Jheng, K.Y. Lu, S.H. Yu, F.L. Mi, Free DOX and chitosan-N-arginine conjugate stabilized indocyanine green nanoparticles for combined chemophotothermal therapy, Colloids Surf. B Biointerfaces 136 (2015) 402–412.

[21] H. Wang, X. Li, B.W.C. Tse, H. Yang, C.A. Thorling, Y. Liu, M. Touraud, J. B. Chouane, X. Liu, M.S. Roberts, X. Liang, Indocyanine green-incorporating nanoparticles for cancer theranostics, Theranostics 8 (2018) 1227–1242.

[22] B.Q. Chen, R.K. Kankala, G.Y. He, D.Y. Yang, G.P. Li, P. Wang, S.B. Wang, Y. S. Zhang, A.Z. Chen, Supercritical fluid-assisted fabrication of indocyanine green-encapsulated silk fibroin nanoparticles for dual-triggered cancer therapy, ACS Biomater. Sci. Eng. 4 (2018) 3487–3497.

[23] C. Ding, J. Gu, X. Qu, Z. Yang, Preparation of multifunctional drug carrier for tumor-specific uptake and enhanced intracellular delivery through the conjugation of weak acid labile linker, Bioconjug. Chem. 20 (2009) 1163–1170.

[24] C.C. Hung, W.C. Huang, Y.W. Lin, T.W. Yu, H.H. Chen, S.C. Lin, W.H. Chiang, H. C. Chiu, Active tumor permeation and uptake of surface charge-switchable theranostic nanoparticles for imaging-guided photothermal/chemo combinatorial therapy, Theranostics 6 (2016) 302–317.

[25] N. Peng, H. Yu, W. Yu, M. Yang, H. Chen, T. Zou, K. Deng, S. Huang, Y. Liu, Sequential-targeting nanocarriers with pH-controlled charge reversal for enhanced mitochondria-located photodynamic-immunotherapy of cancer, Acta Biomater. 105 (2020) 223–238.

[26] T. Yin, Y. Liu, M. Yang, L. Wang, J. Zhou, M. Huo, Novel chitosan derivatives with reversible cationization and hydrophobicization for tumor cytoplasm-specific burst co-delivery of siRNA and chemotherapeutics, ACS Appl. Mater. Interfaces 12 (2020) 14770–14783.

[27] W.H. Jian, T.W. Yu, C.J. Chen, W.C. Huang, H.C. Chiu, W.H. Chiang, Indocyanine green-encapsulated hybrid polymeric nanomicelles for photothermal cancer therapy, Langmuir 31 (2015) 6202–6210.

[28] Z. Yang, N. Sun, R. Cheng, C. Zhao, Z. Liu, X. Li, J. Liu, Z. Tian, pH multistage responsive micellar system with charge-switch and PEG layer detachment for co-delivery of paclitaxel and curcumin to synergistically eliminate breast cancer stem cells, Biomaterials 147 (2017) 53–67.